

Scaling in the Aging Dynamics of the Site-diluted Ising Model

Federico Corberi

*Dipartimento di Fisica “E. R. Caianiello”, and INFN,
Gruppo Collegato di Salerno, and CNISM, Unità di Salerno,
Università di Salerno, via Ponte don Melillo, 84084 Fisciano (SA), Italy.*

Eugenio Lippiello

Dipartimento di Scienze Ambientali, Seconda Università di Napoli, Via Vivaldi, Caserta, Italy

Anupam Mukherjee

CIICA, UAEM, Av. Universidad 1001 Col. Chamilpa, Cuernavaca, Morelos 62210, Mexico

Sanjay Puri

School of Physical Sciences, Jawaharlal Nehru University, New Delhi 110067, India

Marco Zannetti

*Dipartimento di Fisica “E. R. Caianiello”, and INFN,
Gruppo Collegato di Salerno, and CNISM, Unità di Salerno,
Università di Salerno, via Giovanni Paolo II 132, 84084 Fisciano (SA), Italy.*

We study numerically the phase-ordering kinetics of the two-dimensional site-diluted Ising model. The data can be interpreted in a framework motivated by renormalization-group concepts. Apart from the usual fixed point of the non-diluted system, there exist two disorder fixed points, characterized by logarithmic and power-law growth of the ordered domains. This structure gives rise to a rich scaling behavior, with an interesting crossover due to the competition between fixed points, and violation of superuniversality.

I. INTRODUCTION

Relaxation through domain coarsening is a well established paradigm of slow non-equilibrium dynamics. Typically, it takes place in the phase-ordering process following the quench of a system, like a ferromagnet or a binary mixture, to below the critical point [1, 2]. The key feature of coarsening is the unbounded growth of the size $L(t)$ of ordered domains. For large enough times, the existence of a dominant length scale produces an interesting aging-scaling phenomenology in various observable quantities [3–5]. The simplicity of the structure is very attractive and is expected to be valid beyond the realm of disorder-free phase-separating systems. In recent years, this has prompted a considerable effort to understand the role of disorder in systems where its presence does not prevent phase-ordering [6]. Systems of this type are disordered ferromagnets, namely systems where disorder coexists with the low-temperature ferromagnetic order. The unifying theme in this area has been the investigation of the modifications produced by disorder on the properties of the underlying pure systems [6–11].

In our previous works, devoted to the *random-bond Ising model* (RBIM) and the *random-field Ising model* (RFIM) [12–15], we have addressed two long-debated issues. The first one was about the nature of the asymptotic growth law: Power law, with a disorder dependent exponent, against logarithmic behavior. The second was about the so-called *superuniversality hypothesis*, according to which disorder affects the growth law, but not the scaling functions of quantities like correlation and response functions [16]. We have been able to clarify both issues, presenting evidence for an asymptotic logarithmic growth law and for the absence of superuniversal behavior. The achievement of these results has required, in addition to a considerable numerical effort, extensive use of a scaling approach based on the competition between pure and disorder-controlled behavior. The overall picture emerging from our work suggests the existence of an underlying framework, independent of the source of disorder, whose gross common features are: (i) disorder slows down coarsening, producing logarithmic asymptotic behavior; and (ii) the *relevance* of disorder, in a sense to be made precise below, excludes the validity of the superuniversality hypothesis. Differences from system to system arise only in the quantitative details.

In this context, we undertook a study of the two-dimensional *site-diluted Ising model* (SDIM), expecting further confirmation of the above pattern. However, our simulations have revealed a richer phenomenology which is *qualitatively* different from that observed in the RBIM and the RFIM. The major novelty is that, in the SDIM case, more disorder produces slower growth only when disorder is sufficiently small. If the amount of disorder goes beyond a certain threshold, more disorder produces *faster* growth. This lack of monotonicity does not fit into the crossover pattern as observed in the RBIM and RFIM. However, the pieces of what otherwise would be an intricate puzzle,

fall into place if the scaling framework is adequately generalized. Scaling has turned out to be an indispensable tool, without which sorting out the SDIM phenomenology would have been a difficult task.

This paper is organized as follows. The model and the simulations are presented in Section II. The study of the growth law and its scaling analysis are carried out in Sections III and IV. Section V is devoted to the scaling analysis of the autocorrelation function. Finally, in Section VI the conclusions are presented.

II. SITE-DILUTED ISING MODEL

A. Substrate

The substrate is prepared by generating configurations of occupied sites as in random percolation. On the sites of a square two-dimensional lattice there are independent random variables n_i , which take values $n_i = 1$ (occupied site) with probability p and $n_i = 0$ (empty site) with probability $d = 1 - p$. The substrate is formed by the set of occupied sites. In the following, d will be referred to as dilution.

Let us follow the evolution of the geometrical structure of the substrate as dilution is varied from high to low values. We denote the percolation threshold by p_c . Then, for $d > d_c = 1 - p_c \simeq 0.4072$, the substrate is formed by finite clusters of occupied sites. Their characteristic size is

$$\xi(d) \sim |d_c - d|^{-\nu}, \quad (1)$$

where $\nu = 4/3$ and the fractal dimension is $d_f = 91/48$ [17]. The dilution range $d > d_c$ will not be considered in the following since, in the absence of an infinite cluster, coarsening cannot be sustained. At d_c , $\xi(d)$ diverges and an infinite *spanning cluster* is formed. As d is lowered below d_c , the infinite cluster is fractal over distances up to $\xi(d)$, while it becomes compact over larger distances. In addition, finite clusters are also present. This is the structure of the substrate in the dilution regime $d_c \geq d \geq d^*$, where d^* is the special dilution value defined by

$$\xi(d^*) = a, \quad (2)$$

and a is a characteristic microscopic length, like the lattice spacing. For dilutions below d^* , the infinite cluster is compact over all length scales and there are no finite clusters. There remain vacancies inside the infinite cluster which are essentially single-site vacancies. Hence, in the dilution regime $d^* \geq d \geq 0$, the average distance between pairs of vacancies defines a new characteristic length

$$\lambda(d) = a(d/d^*)^{-1}. \quad (3)$$

B. Spin System

The SDIM is obtained by putting Ising spins $\sigma_i = \pm 1$ on the substrate or, equivalently, on the whole lattice and taking an interaction Hamiltonian of the form

$$H = -J \sum_{\langle ij \rangle} n_i n_j \sigma_i \sigma_j. \quad (4)$$

Here, $\langle ij \rangle$ denotes nearest-neighbour pairs, and $J > 0$ is a ferromagnetic coupling constant. The variables $\{n_i\}$ enter the problem as quenched disorder.

1. Equilibrium States

For $d \leq d_c$, at low enough temperature the system exhibits ferromagnetic order. In the (d, T) plane there is a critical line $T_c(d)$, which separates the paramagnetic from the ferromagnetic phase. The equilibrium phase diagram is pictorially represented in Fig. 1. The critical temperature, which in the following will be measured in units of k_B/J , where k_B is the Boltzmann constant, decreases from the pure Ising model value [$T_c(0) \simeq 2.269$] as the dilution is increased and vanishes at d_c [$T_c(d_c) = 0$] since the structure is disconnected for $d > d_c$.

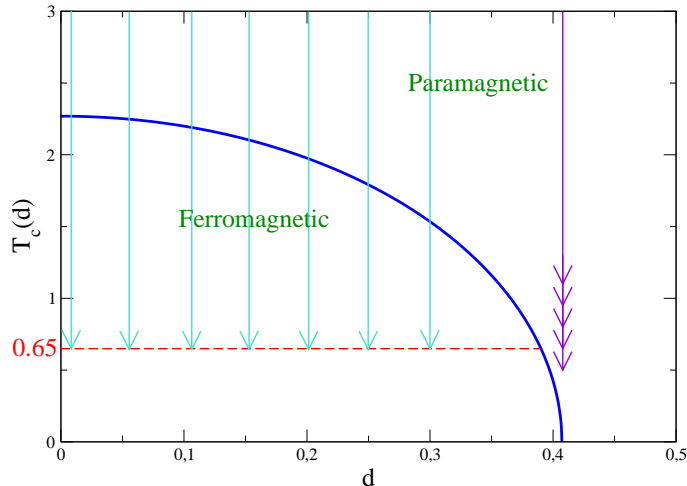


FIG. 1: Pictorial representation of the equilibrium phase diagram of the SDIM. The bold blue line is the critical temperature $T_c(d)$. The temperature $T = 0.65$ where most simulations will be performed is marked with a red line. Vertical arrows represent the quenching processes considered in the simulations.

2. Time Evolution

The occupied sites evolve with non-conserved dynamics [1, 2]. We use single-spin-flip transition rates of the Glauber form

$$w(\sigma_i \rightarrow -\sigma_i) = \frac{1}{2} [1 - \sigma_i \tanh(H_i^W/T)]. \quad (5)$$

Here, H_i^W is the local Weiss field obtained by the sum

$$H_i^W = \sum_{j \in L_i} n_j \sigma_j \quad (6)$$

over the set of nearest-neighbors L_i of i . We consider a cooling procedure where the system is prepared initially in the infinite-temperature disordered state. At the time $t = 0$, it is suddenly quenched to a finite temperature T . We will study the following two classes of quenches:

- (i) The dilution of the system is in the range $d \in [0, 0.3]$ and the final temperature is $T = 0.65$ (represented by the cyan vertical arrows in Fig. 1).
- (ii) We have $d = d_c$ and different values of $T > 0$ (represented by the violet arrows in Fig. 1).

In the first case, the system is always quenched well below the critical temperature $T_c(d)$ [18], as sketched in Fig. 1. In this situation, one can speed up the simulations by using a modified dynamics where spin flips in the bulk of domains, namely those aligned with all the nearest neighbors, are prevented. This modified dynamics does not alter the behavior of the quantities we are interested in, as has been tested in a large number of cases [19]. We have checked that this is also true in the present study.

In the second case, the system is quenched to finite temperatures, because at $T = 0$ the evolution gets frozen in metastable states and there is no long-time dynamics. Hence we are quenching above the critical temperature $T_c(d_c) = 0$ and the system will eventually relax to a disordered state with a finite spin coherence length $\xi_\sigma(T)$ [not to be confused with the substrate property $\xi(d)$]. However, since $\xi_\sigma(T)$ diverges very fast for $T \rightarrow 0$, a coarsening phenomenon is seen in the pre-asymptotic stage. The corresponding growth of $L(t)$ will eventually end at $t = t_{eq}(T)$ when $L(t) \simeq \xi_\sigma(T)$. The situation is similar to the one found in other ferromagnetic systems with $T_c = 0$ as, for instance, the one-dimensional Ising model with conserved dynamics [20]. In order to study the ordering phenomenon, we have set T sufficiently low as to never observe the equilibration of the system. Further, it can be shown that flips of bulk spins are only observed for $t \gtrsim t_{eq}(T)$, so we use the modified dynamics discussed above in this case also.

3. Simulation Details

The details of the simulations are as follows. We have considered a two-dimensional square lattice system of $N = 2000^2$ lattice sites. We have checked that, with this choice, no finite-size effects can be detected in the time-regime accessed by the simulations. For every choice of the parameters, we perform a certain number (in the range 10-100) of independent runs with different initial conditions and thermal histories in order to populate the non-equilibrium ensemble needed to extract average quantities that will be introduced below.

C. Observables

The two observable quantities of interest in this paper are the typical domain size $L(t)$ and the autocorrelation function:

$$C(t, t_w) = \frac{1}{N} \sum_{i=1}^N [\langle \sigma_i(t) n_i \sigma_i(t_w) n_i \rangle - \langle \sigma_i(t) n_i \rangle \langle \sigma_i(t_w) n_i \rangle], \quad (7)$$

where t, t_w ($0 < t_w < t$) are a pair of times after the quench. The angular brackets denote a non-equilibrium ensemble average, taken over random initial conditions and over dynamical trajectories.

For a model defined on a disconnected substrate, as it happens for $d > d^*$, phase ordering occurs independently on the various parts of the system and, correspondingly, different definitions of the growing length can be given. Indeed, while on the spanning cluster growth continues indefinitely, on finite clusters it saturates to their size. Since we are interested in the aging phenomenon related to the existence of a divergent length, we define $L(t, d)$ as the characteristic length of the ordered regions which are effectively growing. As we will discuss soon, this quantity can be computed as the inverse excess energy:

$$L(t, d) = [E(t, d) - E_\infty(d)]^{-1}. \quad (8)$$

Here, $E(t, d) = \langle H(t) \rangle$ is the energy at time t , and $E_\infty(d)$ is the energy of the equilibrium state at the final temperature T . Equation (8) is often used to determine $L(t)$ in non-diluted systems [1]. It expresses the simple fact that the excess energy of the coarsening system with respect to the equilibrated one is associated with the density of domain walls. This, in turn, is inversely proportional to the typical domain size. Besides its simplicity, in the diluted case the definition (8) has the further advantage that the disconnected finite parts of the substrate which are already ordered do not contribute to the computation of $L(t, d)$. Indeed a finite cluster is by definition surrounded by empty sites and hence there is no excess energy associated with it when its spins are aligned.

III. GROWTH LAW

The time dependence of $L(t, d)$, for the three dilution values $d = 0, d^* = 0.225, d_c$, is plotted in the upper panel of Fig. 2. Here d^* is identified as the dilution value corresponding to the slowest numerically observed asymptotic growth. The connection with the dilution d^* of Eq. (2) will be clear below. The plot shows that disorder is a relevant perturbation with respect to pure behavior, since for $d > 0$ the late time growth is considerably slower than the pure-like power law. However, contrary to what is observed in the Ising model with random bonds and random fields [7–15], Fig. 2 shows, as anticipated in the Introduction, that the d -dependence of $L(t, d)$, at fixed time t , is non-monotonic. The nature of the problem can be grasped at glance by looking at the lower panel of Fig. 2, which has been produced by a fine sampling of the dilution range $[0, d_c]$. In the three-dimensional plot the growth law appears as a surface with the shape of an upward bending valley. The growth-law of the pure system, denoted as $L_0(t)$ is marked in the figure with a bold blue line. This is the case where the growth is faster, as it can be clearly seen, in agreement with the general observation that, particularly at low T , the dynamics of a disordered system is slower than in the corresponding pure one, because disorder pins the interfaces. Naively one could also expect that the kinetics gets slower and slower as the parameter that controls the strength of the disorder (in this case d) is increased, as it is generally observed in various disordered ferromagnetic models [7–15, 21, 22]. This feature is also found in the present system, but only when the dilution is increased from zero up to $d = d^*$. The growth-law at this density is marked by the bold dark line at the bottom of the valley in the figure. For $d > d^*$ growth increases again up to the bold yellow line corresponding to $L(t, d_c)$. The non-monotonous character of the growth law, for fixed t , corresponds to descending toward the bottom of the valley and then climbing again as d is varied. This non-monotonicity prevents the explanation of the data within the straightforward scaling framework arising from the competition between an

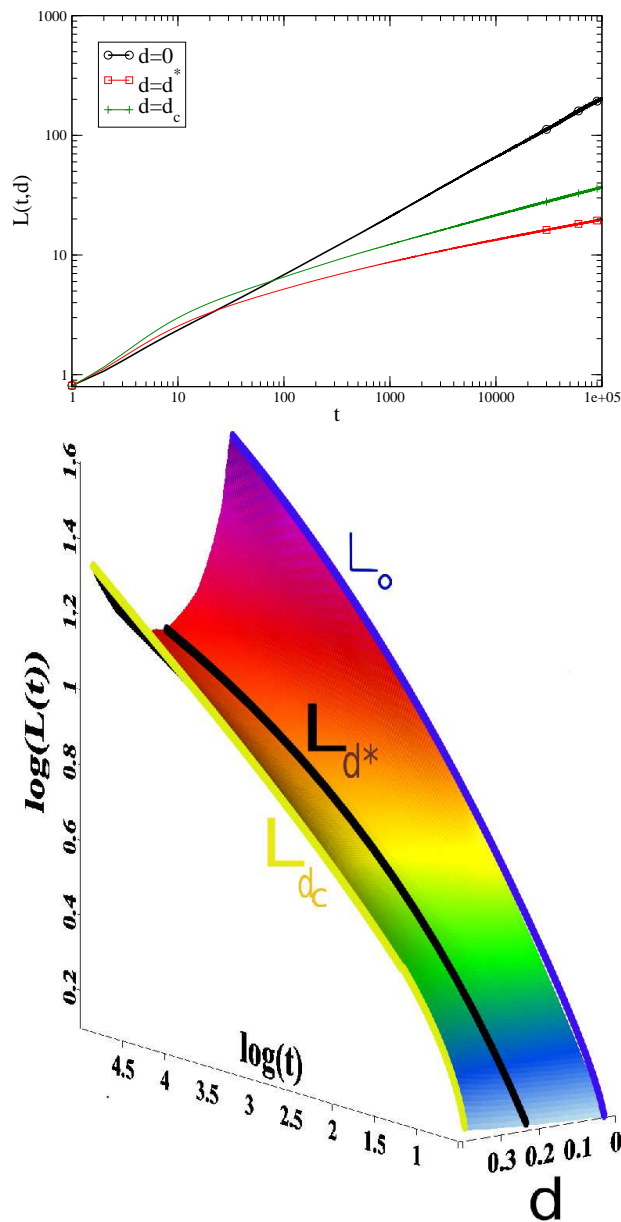


FIG. 2: The behavior of the typical length $L(t)$ after a quench to $T = 0.65$ is shown in the upper panel for the three dilutions $d = 0, d = d^*$ and $d = d_c$ in a double logarithmic plot. In the lower panel the same quantity is shown in a three-dimensional plot as t and d are varied. Color code is from light blue ($L(t, d)$ very small) to violet ($L(t, d)$ very large). The three bold lines are the curves for $d = 0, d = d^*, d = d_c$ plotted in the upper panel.

unstable pure fixed point and a stable disorder-controlled fixed point [13–15]. In the next section we shall develop the scaling approach required by the above phenomenology.

IV. SCALING

From the discussion of the substrate made in subsection II A, the three dilutions $d = 0, d = d^*, d = d_c$ emerge as special values, since the asymptotic states toward which the system evolves are scale-free, in the sense that all lengths involved are either zero or infinite. Clearly, $L(t, d)$ diverges in all cases as $t \rightarrow \infty$. In addition $\lambda(0) = \infty$, $\xi(d_c) = \infty$ and, at d^* , both $\xi(d^*)$ and $\lambda(d^*)$ are of the order of the microscopic length a , which for the sake of simplicity we shall

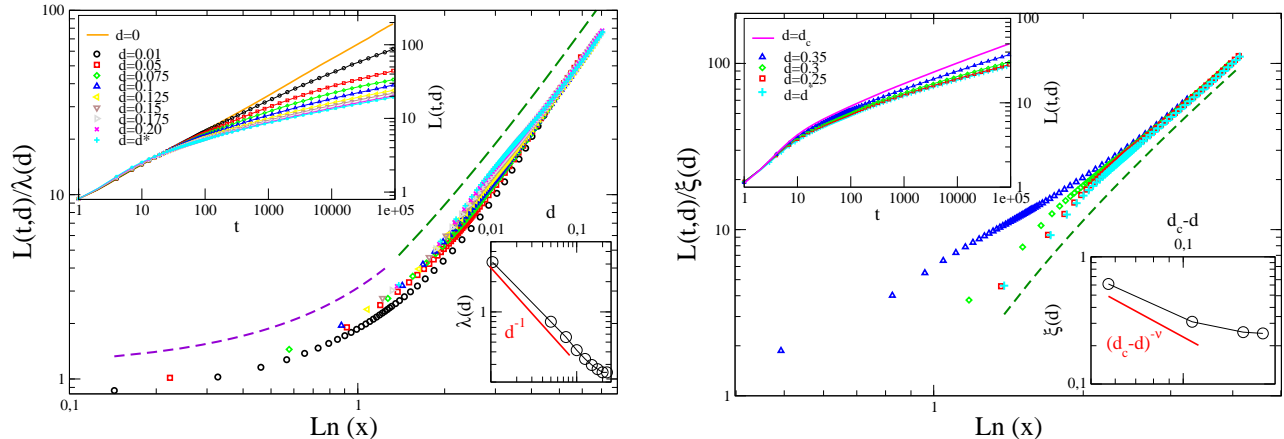


FIG. 3: In the upper insets the raw data for $L(t, d)$ are plotted for quenches at $T = 0.65$ and various $0 \leq d \leq d^*$ (left panel) or $d^* \leq d \leq d_c$ (right panel) in a log-log plot. In the main figures the scaling functions ℓ (left panel) and \mathcal{L} (right panel) are plotted in a log-log plot against $\ln x$, where $x = t^{1/z}/\lambda(d)$ (left panel) or $x = t^{1/\zeta(T)}/\xi(d)$ (right panel). The dashed violet and green lines are the fitting curves $y \propto x$ and $y = (a + b \ln x)^{1/\psi}$ with $x = t^{1/z}/\lambda(d)$ and the values of a, b, ψ given in the text (the curves have been vertically displaced for clarity). The lower insets show the dependence of the rescaling parameter $\lambda(d)$ and $\xi(d)$ on d . The bold red lines are the expected behaviors, respectively Eq. (3) and Eq. (1).

now treat as negligible, that is $\xi(d^*) \simeq \lambda(d^*) \simeq 0$. Therefore, the three dilutions $d = 0, d = d^*, d = d_c$ are candidates for fixed points, in the renormalization group (RG) sense of the word, lying on the dilution axis.

If this was correct, the growth law for d other than a fixed point value ought to exhibit crossover from the pre-asymptotic behavior, characteristic of the nearby unstable fixed point, to the asymptotic behavior characteristic of the nearby stable fixed point. Indeed, this is what happens.

A. Small Dilution: $0 \leq d \leq d^*$

Let us consider first the dilution regime $0 \leq d \leq d^*$, which will be referred to as small dilution. Assuming scaling and recalling that in the pure case

$$L(t, 0) \sim t^{1/z} \quad (9)$$

with $z = 2$, the growth law can be written in the form

$$L(t, d) = \lambda(d) \ell \left(\frac{t^{1/z}}{\lambda(d)} \right). \quad (10)$$

According to the assumption, the data obtained for different values of d should collapse on a single master curve $\ell(x)$ by plotting $L(t, d)/\lambda(d)$ against $x = t^{1/z}/\lambda(d)$. This is shown in the left panel of Fig. (3). The upper inset displays the raw data in a log-log plot: The upper straight line is the power law (9) of the pure case. As d is increased from zero, growth slows down and converges toward $L(t, d^*)$, which is the slowest growth. Extracting empirically the length $\lambda(d)$ (lower inset) the data can be collapsed, as depicted in the main panel.

The master curve in the left panel of Fig. 3 grows linearly in x for $1 \gtrsim x$ and can be fitted with the curve $y = (a + b \ln x)^{1/\psi}$ with $a = 0.3232$, $b = 0.5325$, and $1/\psi = 2.3545$ in the region $x \gtrsim 1$. In conclusion

$$\ell(x) \sim \begin{cases} (\ln x)^{1/\psi} & , \quad \text{for } x \gg 1, \\ x & , \quad \text{for } x \ll 1. \end{cases} \quad (11)$$

This shows that the pure-like behavior of Eq. (9) is unstable to disorder perturbation and that the d^* -behavior

$$L(t, d^*) \sim \lambda(d) (\ln t)^{1/\psi}, \quad (12)$$

with $1/\psi \simeq 2.35$, is asymptotically dominant for all d in the range $(0, d^*]$. The logarithmic behavior (12) is in contrast with the results of Ref. [9], where data are interpreted as power law growths for any d , while it agrees with results for small dilutions of Ref. [22] (although a slightly larger exponent $1/\psi \simeq 2.5$ is reported). The discussion above shows that $d = 0$ and d^* can be identified, respectively, with the unstable and the stable fixed point in the small dilution regime. Notice (lower inset of the left panel in Fig. 3) that $\lambda(d) \sim d^{-1}$ as $d \rightarrow 0$, in agreement with the behavior expected from Eq. (3), and that the collapse is not perfect. The spread of the curves for $x \ll 1$ reveals the existence of a correction to scaling due to the microscopic length a introduced in Eq. (2). a enters the scaling function of Eq. (10) through an extra variable $t^{1/z}/a$, which does not appear explicitly in order to keep a compact notation. Since generally $a \ll \lambda(d)$ this term produces corrections at small times, as we observe in Fig. 3.

B. Large Dilution: $d^* \leq d \leq d_c$

Let us first of all recall the discussion of Sec. II B 2 according to which all the quenches with $d < d_c$ are below the critical temperature while in the quench with $d = d_c$ we consider the pre-asymptotic phase-ordering stage preceding equilibration in a disordered state. This being said, a scaling analysis analogous to the previous one can be carried out in the large dilution regime $d^* \leq d \leq d_c$. Looking at the raw data in the upper inset of the right panel of Fig. 3, the fastest growth occurs at d_c , slowing down as d decreases and converging toward $L(t, d^*)$, which is again the slowest growth. Therefore, in the large dilution regime the unstable fixed point is at d_c , while d^* is still the attractive fixed point, being stable with respect to perturbations from both the small and the high dilution side. As shown in Fig. 4, right at d_c the growth law obeys the power law (see Fig. 4)

$$L(t, d_c) \sim t^{1/\zeta(T)}, \quad (13)$$

where $\zeta(T) > 2$ is a temperature-dependent exponent. For low temperatures, this behaves as

$$\zeta(T) \sim T^{-1}. \quad (14)$$

An argument to explain these facts will be presented below in Sec. IV C.

Recalling that in the large dilution regime the characteristic length is given by $\xi(d)$, the scaling form of the growth law, analogous to Eq. (10), is given by

$$L(t, d) = \xi(d) \mathcal{L} \left(\frac{t^{1/\zeta(T)}}{\xi(d)} \right), \quad (15)$$

where the chosen value of the final temperature T enters explicitly through $\zeta(T)$. This is checked following the same procedure as above. After extracting the length $\xi(d)$ (see lower inset in the right panel of Fig. 3), the collapse of the data is displayed in the main panel, with the master curve obeying limiting behaviors analogous to those in Eq. (11)

$$\mathcal{L}(x) \sim \begin{cases} (\ln x)^{1/\psi} & , \quad \text{for } x \gg 1, \\ x & , \quad \text{for } x \ll 1, \end{cases} \quad (16)$$

where now $x = t^{1/\zeta(T)}/\xi(d)$, and $1/\psi \simeq 2.35$.

C. An Argument for $L(t, d)$

In this section we present an argument which explains the growth-laws observed. We start with the case $d = d_c$, focusing the attention on the fractal spanning cluster, a portion of which is schematically sketched in Fig. 5.

The six panels represent different snapshots of the system while it is progressively crossed by an interface. Up spins are colored in blue while the down ones are red. Initially, at some time t_0 (up-left panel), the interface is located on the very left of the figure, and then it moves to the right at the subsequent times $t_0 + \tau_0 < t_1 < t_1 + \tau_1 < t_2 < t_2 + \tau_2$ represented in the other panels. The cutting bonds [17], namely those links whose removal causes disconnection, are represented as lines connecting *bulky* regions, free of cutting bonds, represented by squares. Let us denote with L_1 the size of the down spin domain at time t_1 and with L_2 that at $t = t_2$. One has $L_2 = kL_1$ ($k = 2$ in the figure) or, in general, defining L_m as the size at time t_m ,

$$L_m = kL_{m-1}. \quad (17)$$

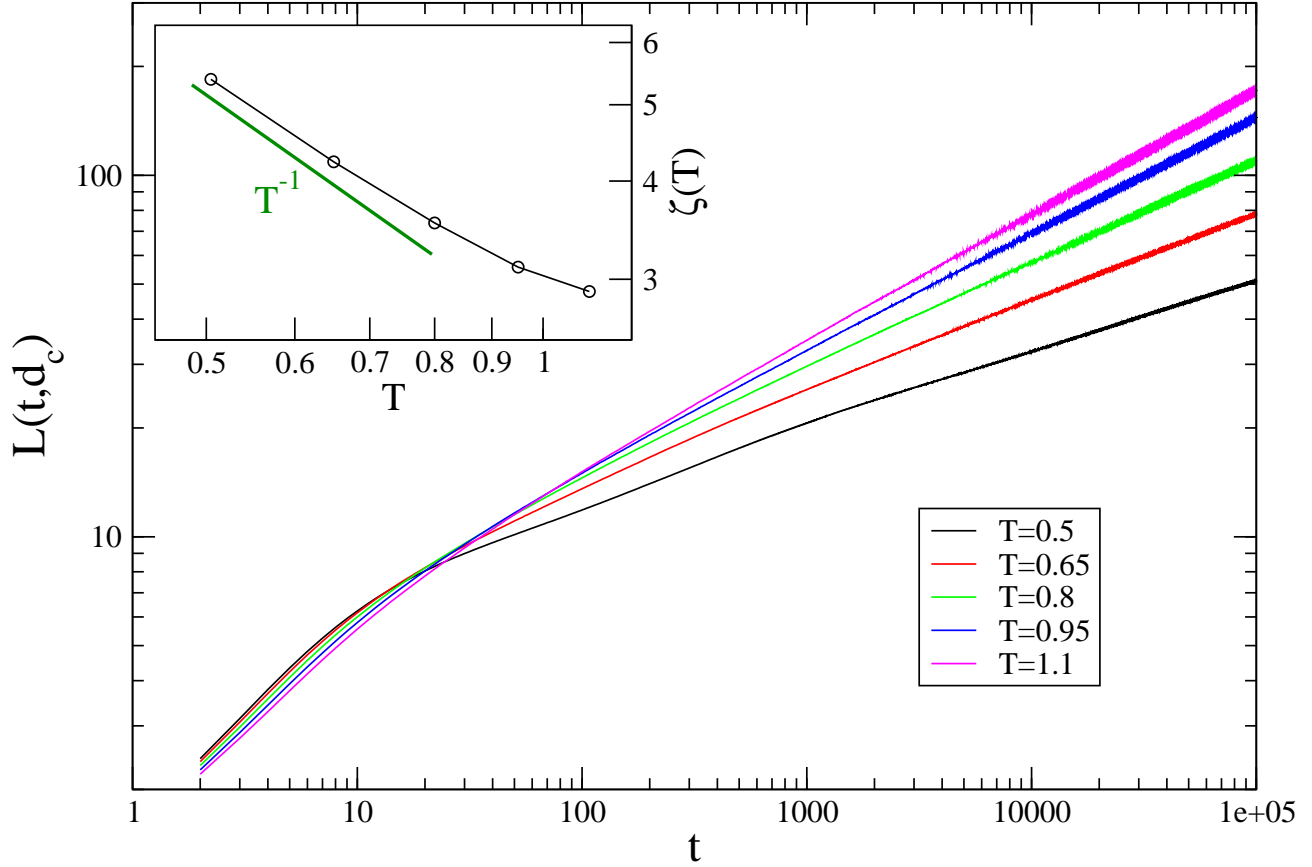


FIG. 4: $L(t, d_c)$ is plotted against t in a quench at different temperatures (see key). In the inset $\zeta(T)$ (obtained as the best fit of the curves in the large- t sector) is plotted against T in a double logarithmic graph. The bold green line is the law T^{-1} .

Analogously, by counting the number of down spins N_1 (N_2) at $t = t_1$ (t_2) one has $N_2 = nN_1$ ($n = 3$ in the figure) and, in general, $N_m = nN_{m-1}$. This implies that the fractal dimension d_f of the substrate defined by $N_m \propto L_m^{d_f}$ is $d_f = \ln n / \ln k$.

We now want to study the energetic barriers that the interface has to overcome while moving. The highest energy E_1^{max} (E_2^{max}) of the interface in the time interval $[t_0, t_1]$ ($[t_1, t_2]$) will occur at some intermediate time $t_0 + \tau_0$ ($t_1 + \tau_1$), as sketched in the figure. Notice that, in going from t_1 to t_2 , the two bulky regions can be crossed one after the other. This implies $E_2^{max} \simeq E_1^{max} + qJ$ because at time $t_1 + \tau_1$ there is an energy E_1^{max} associated to the piece of interface spanning the upper bulky region, as at $t = t_0 + \tau_0$ (we make the assumption that bulky regions are equivalent) but an extra bond (q bonds in a more generic network) with misaligned spins is present (the one connecting the lower bulky region), with an associated energy J . Generalizing the above result to a generic step one has $E_m^{max} = E_m^{max} + qJ$. The height of the energetic barrier in going from t_m to t_{m+1} is given by $\Delta E_m = E_m^{max} - E_m^{min}$, where the minimum energy of the interface E_m^{min} is taken at t_m and at t_{m+1} and it does not depend on m because there is always the same number of broken bonds in these states. This implies

$$\Delta E_{m+1} = \Delta E_m + qJ. \quad (18)$$

Expressing m in terms of the size L_m through Eq. (17), and dropping the index m (i.e. posing $L_m = L$) we can write $\Delta E(kL) = \Delta E(L) + qJ$. Solving we find scaling of the barriers with L as

$$\Delta E(L) = a \ln L, \quad (19)$$

with $a = qJ / \ln k$. Finally, using the Arrhenius law $t \sim e^{\Delta E / (k_B T)}$ for the time needed to exceed an energetic barrier ΔE we arrive at

$$L(t) \propto t^{1/\zeta(T)}, \quad (20)$$

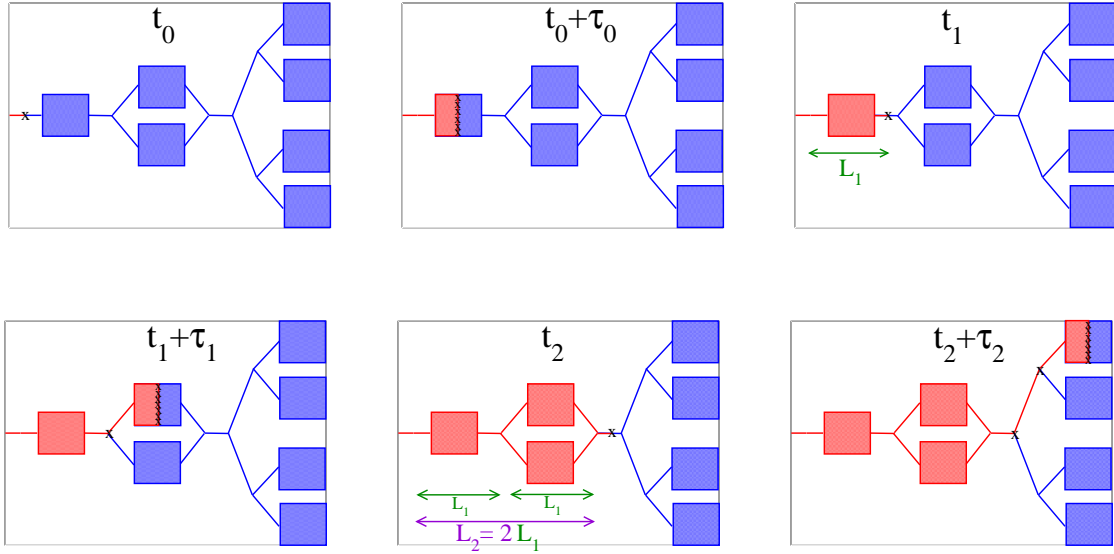


FIG. 5: Schematic representation of coarsening on the percolation network. An x represents an unsatisfied bond.

with

$$\zeta(T) = \frac{a}{k_B T}, \quad (21)$$

which agree with Eqs. (13,14).

The situation is different for $d < d_c$, because here the cutting bonds are absent. In order to represent schematically this property we increase the connectivity of the substrate of Fig. 5 in such a way that any bulky region is directly connected by q link with the others, as shown in Fig. 6 (where $q = 1$).

Starting from a configuration of minimum energy $E_1^{min} = 2qJ$ at time t_1 one arrives to a maximum $E_1^{max} = 4qJ$ at time $t = t_1 + \tau_1$. Then the new minimum with $E_2^{min} = 4qJ$ is reached at t_2 , followed by the next maximum of energy $E_2^{max} = 8qJ$ at $t = t_2 + \tau_2$. On a generic structure, for a generic m one has $E_m^{min} = K^m qJ$ and $E_m^{max} = bK^m qJ$, where K describes how the number of links increases as the interface spans the structure and b is a constant ($K = 2$ and $b = 2$ in the figure). Hence $\Delta E_m = (b - 1)K^m qJ$. Then, due to the modified connectivity of the network, in place of Eq. (18) one has

$$\Delta E_{m+1} = \Delta E_m + (b - 1)(K - 1)K^m qJ, \quad (22)$$

leading to $\Delta E(kL) = \Delta E(L) + (b - 1)(K - 1)(L/L_0)^\psi qJ$, with $\psi = (\log_K k)^{-1}$, from which

$$\Delta E(L) = aL^\psi, \quad (23)$$

where $a = (b - 1)(K - 1)qJ/[L_0^\psi(K^\psi - 1)]$. Using the Arrhenius law, one arrives at

$$L(t, d < d_c) \propto (\ln t)^{1/\psi}, \quad (24)$$

in agreement with Eq. (12). Notice that, in the present approach, the striking difference between the two growth laws (20) and (24) is due to the different topological features of the substrate right at $d = d_c$ or for $d < d_c$, specifically due to the presence/absence of cutting bonds.

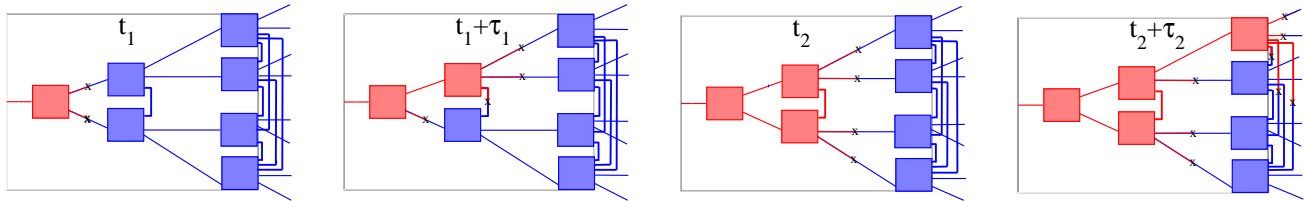


FIG. 6: Schematic representation of coarsening on the network with $d < d_c$.

V. AUTOCORRELATION FUNCTION

Scaling is expected to hold for any other observable quantity. In particular, for the autocorrelation function (7) we expect

$$C(t, t_w, d) = \begin{cases} c\left(\frac{L(t)}{L(t_w)}, \frac{\lambda(d)}{L(t_w)}\right) & , \quad \text{for } d \leq d^* \\ \mathcal{C}\left(\frac{L(t)}{L(t_w)}, \frac{\xi(d)}{L(t_w)}\right) & , \quad \text{for } d \geq d^*, \end{cases} \quad (25)$$

with the limiting forms of the scaling functions

$$c(x, y) = \begin{cases} C_0(x) & , \quad \text{for } y \rightarrow \infty \\ C_{d^*}(x) & , \quad \text{for } y \rightarrow 0 \end{cases} \quad (26)$$

and

$$\mathcal{C}(x, y) = \begin{cases} C_{d_c}(x) & , \quad \text{for } y \rightarrow \infty \\ C_{d^*}(x) & , \quad \text{for } y \rightarrow 0. \end{cases} \quad (27)$$

Here $C_0(x)$ is the thoroughly studied scaling function of the pure system [1, 23, 24], while $C_{d^*}(x)$ and $C_{d_c}(x)$ are the scaling functions at the other two fixed points which, as far as we know, have not been studied before. Notice the absence of powers of L in front of the scaling functions. As it is well known [25], this is due to the fact that domains grow compactly on the substrate, even if the substrate itself, as at the percolation threshold d_c , may be a fractal.

According to the scaling forms above, if the dilution is set exactly at the fixed point values $d = 0, d = d^*, d = d_c$, where either $\lambda(d) = 0$ or $\lambda(d) = \infty$, or $\xi(d) = \infty$, the autocorrelation function should depend only on $x = L(t)/L(t_w)$ when t_w is sufficiently large. This prediction is checked in Fig. 7 where, for these three special dilutions the expected data collapse is obtained by plotting C against x . In the case with $d = 0$ (lower set of curves) one recovers the well known result [1, 23] of a convergence towards data collapse in the large- t_w limit. Poor data collapse at early t_w is a feature related to the pre-asymptotic corrections to scaling due to the microscopic length a [1, 23]. By contrast, at d^* (set of curves in the middle) and at $d = d_c$ (upper set of curves), an excellent data collapse is obtained even for moderate values of t_w . For any value of $x > 1$ the fixed point scaling functions satisfy the inequality

$$C_0(x) < C_{d^*}(x) < C_{d_c}(x). \quad (28)$$

Next, let us look at dilutions other than the fixed point values. The two cases, the first with $0 < d < d^*$ and the second with $d^* < d < d_c$, are depicted in Fig. 8 (left and central panel). Here we find that, at variance with the fixed point cases, the curves for different t_w do not collapse. However, in both cases as t_w is increased the curves tend to the scaling function $C_{d^*}(x)$ of the attractive fixed point at d^* (from below and from above, respectively). Given the inequality (28), these behaviors imply that $c(x, y)$ and $\mathcal{C}(x, y)$ are slowly crossing over from the pre-asymptotic forms $C_0(x)$ and $C_{d_c}(x)$ (respectively) at early t_w , to the asymptotic one $C_{d^*}(x)$ as y is varied. This is a clear-cut confirmation of the crossover pattern uncovered from the study of the growth law in Sec. IV.

An alternative representation of crossover is given in the right panel of Fig. 8. Here $C(t, t_w, d)$ is plotted against t_w for fixed $x = t/t_w$ and for different dilution values spanning the whole range $[0, d_c]$. At the three fixed point ($d = 0, d^*, d_c$) the curves converge toward the respective asymptotic values. For values of d different from these, the curves are asymptotically attracted toward the one corresponding to d^* . Notice that, for values of d sufficiently close to d_c (as for the case $d = 0.35$), the pre-asymptotic behavior corresponding to the nearby unstable fixed point

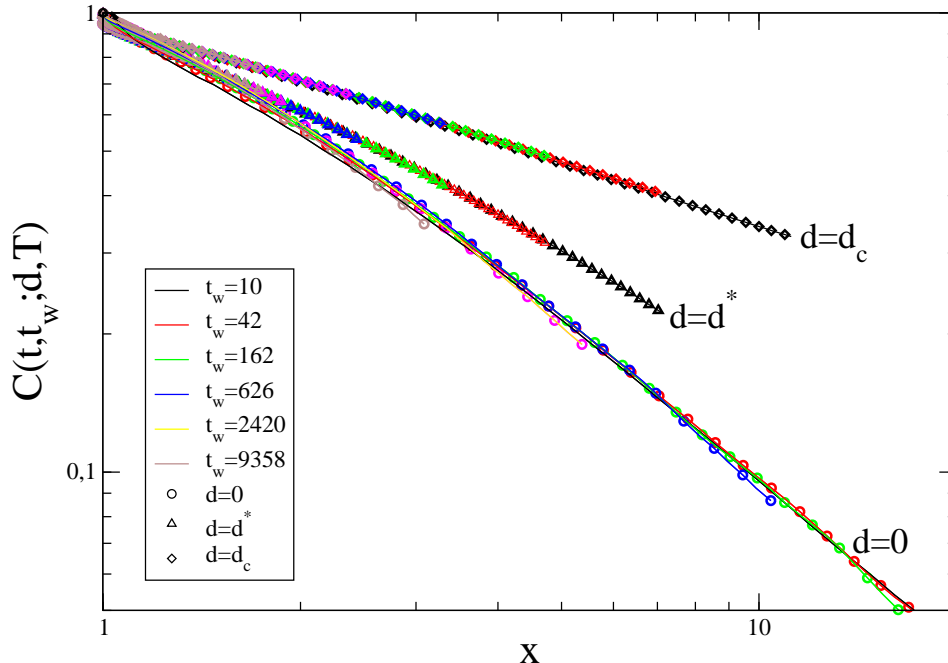


FIG. 7: Data collapse of $C(t, t_w; d)$ against $x = L(t)/L(t_w)$, for different values of t_w (see caption), for a quench to $T = 0.65$ and the three fixed point dilutions $d = 0$ (lower curves), $d = d^*$ (central curves), $d = d_c$ (upper curves).

is observed. Indeed, the curve initially increases (towards the plateau value of the case $d = d_c$), and then decreases towards the value of the $d = d^*$ case.

Let us stress that, due to the presence of the variable $y = \lambda(d)/L(t_w)$ (or $\xi(d)/L(t_w)$) in Eq. (25) the autocorrelation function is a function of $x = L(t)/L(t_w)$ only if d is set to one of the fixed point densities where y vanishes or diverges. Conversely, in Ref. [22] collapse of the curves for the autocorrelation is found when plotted against x at any value of d . This can be perhaps understood as due to the large values of t_w used in Ref. [22]. It must be recalled in fact that in the large- t_w limit the curves approach the master curve C_{d^*} of the attractive fixed point, and it may be numerically hard to detect the dependence on y . However the dependence on y implied by the scaling picture is present, as it is clearly visible in Fig. 8. Moreover at least in one case the results of [22] are obtained for a value ($d = 0.2$) of the dilution so close to d^* to basically probe the scaling at d^* where indeed there is no further dependence on y .

Finally, notice that the scaling behavior of the autocorrelation discussed insofar excludes superuniversality, since the three scaling functions C_0 , C_{d^*} and C_{d_c} are different, depend on the disorder strength d , and obey the inequality (28).

VI. DISCUSSION AND CONCLUSIONS

In this paper, we have studied the phase-ordering kinetics of the two-dimensional diluted Ising model. Numerical data can be consistently interpreted in a RG-inspired scaling scheme with three fixed points (FPs): an attractive FP at $d = d^*$ and two repulsive FPs at the limits $d = 0$ and $d = d_c$ of the possible dilution values. This structure can be geometrically interpreted as due to the existence of two sectors separated by d^* : for $d < d^*$, vacancies play the role of isolated voids separated by a distance $\lambda(d) \propto d^{-1}$, whereas for $d > d^*$, the spin network has a percolative fractal structure up to distances $\xi(d) \propto (d_c - d)^{-\nu}$. At d^* these two lengths become microscopic and merge, while they respectively diverge at $d = 0, d_c$, providing in this way three FPs for the dynamics and an associated pattern of crossovers regulated by their attractive/repulsive character. This behavior excludes superuniversality, as has been clearly shown when discussing the properties of the autocorrelation function.

As a final observation let us comment on the fact that, at least at d_c , the growth law of the domains can be

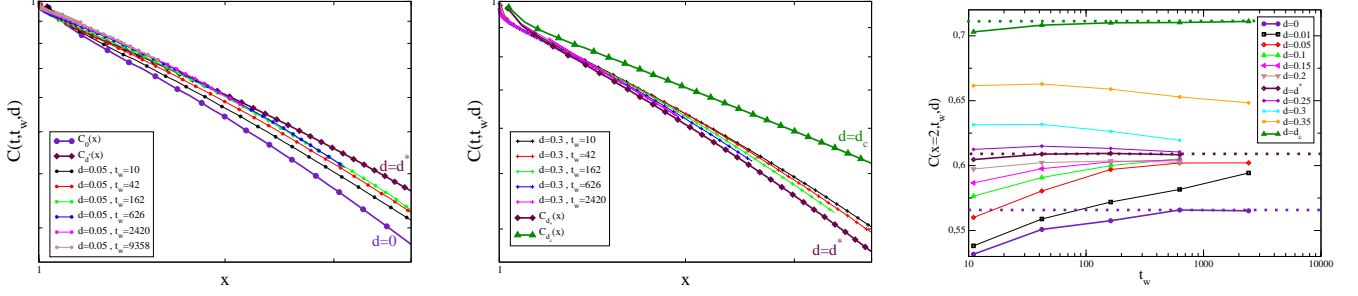


FIG. 8: $C(t, t_w; d)$ is plotted against against $x = t/t_w$ for different choices of t_w (see caption) in a quench to $T = 0.65$ and $d = 0.05$ (left panel), and $d = 0.3$ (central panel). The bold curves with heavy symbols are the scaling functions $C_0(x)$, $C_{d^*}(x)$, $C_{d_c}(x)$ (see caption). In the right panel we plot $C(t, t_w; d, T)$ against t_w by fixing $x = t/t_w = 2$ in quenches to different values of d (see caption) spanning the entire range $[0 - d_c]$. The bold dashed lines are guide to the eye representing the asymptotic values $\lim_{t_w \rightarrow \infty} C(x = 2, t_w, d = 0)$, $\lim_{t_w \rightarrow \infty} C(x = 2, t_w, d = d^*)$, $\lim_{t_w \rightarrow \infty} C(x = 2, t_w, d = d_c)$ (from bottom to top).

understood in terms of topological properties of the spin network as, in particular, the weakness of the fractal graph due to the presence of the cutting bonds. Although the argument presented in Sec. IV C has been developed for $L(t)$, we expect that the role played by the topology might affect other observables. This observation provides a link between the actual system and the related problem of phase-ordering on fractal structures where the importance of analogous topological properties has been pointed out [26]. One might ask if the role of topology could have important consequences also in ferromagnets with a different kind of disorder, as for instance random bonds.

-
- [1] A.J. Bray, *Adv. Phys.* **43**, 357 (1994).
 - [2] S. Puri, in *Kinetics of Phase Transitions*, edited by S. Puri and V. Wadhawan, CRC Press, Boca Raton (2009), p. 1.
 - [3] M.Zannetti, in *Kinetics of Phase Transitions* (Ref. [2]), p.153.
 - [4] J.P.Bouchaud, L.F.Cugliandolo, J.Kurchan and M.Mezard, in *Spin Glasses and Random Fields*, edited by A.P.Young (World Scientific, Singapore, 1997).
 - [5] F. Corberi, L. F. Cugliandolo, and H. Yoshino, in *Dynamical Heterogeneities in Glasses, Colloids, and Granular Media*, edited by L. Berthier, G. Biroli, J.-P. Bouchaud, L. Cipelletti, and W. Van Saarloos (Oxford University Press, Oxford, 2011).
 - [6] S. Puri, *Phase Transitions* **77**, 469 (2004).
 - [7] S. Puri, D. Chowdhury and N. Parekh, *J. Phys. A* **24**, L1087 (1991); S. Puri and N. Parekh, *J. Phys. A* **25**, 4127 (1992).
 - [8] A.J. Bray and K. Humayun, *J. Phys. A* **24**, L1185 (1991).
 - [9] R. Paul, S. Puri and H. Rieger, *Europhys. Lett.* **68**, 881 (2004); R. Paul, S. Puri and H. Rieger, *Phys. Rev. E* **71**, 061109 (2005); R. Paul, G. Schehr and H. Rieger, *Phys. Rev. E* **75**, 030104(R) (2007).
 - [10] M. Henkel and M. Pleimling, *Europhys. Lett.* **76**, 561 (2006); *Phys. Rev. B* **78**, 224419 (2008).
 - [11] A. Sicilia, J. J. Arenzon, A. J. Bray and L. F. Cugliandolo, *Europhys. Lett.* **82**, 1001 (2008); M. P. O. Loureiro, J. J. Arenzon, L. F. Cugliandolo, and A. Sicilia, *Phys. Rev. E* **81**, 021129 (2010).
 - [12] F. Corberi, A. de Candia, E. Lippiello and M. Zannetti, *Phys. Rev. E* **65**, 046114 (2002); F. Corberi, A. de Candia, E. Lippiello and M. Zannetti, *Physica A* **314**, 454 (2002).
 - [13] E. Lippiello, A. Mukherjee, S. Puri and M. Zannetti, *Europhys. Lett.* **90**, 46006 (2010).
 - [14] F. Corberi, E. Lippiello, A. Mukherjee, S. Puri and M. Zannetti, *J. Stat. Mech.: Theory and Experiment* P03016 (2011).
 - [15] F. Corberi, E. Lippiello, A. Mukherjee, S. Puri, and M. Zannetti, *Phys. Rev. E* **85**, 021141 (2012).
 - [16] L.F. Cugliandolo, *Physica A* **389**, 4360 (2010). For an explanation of the superuniversality concept see Sec. 5.2 and references quoted therein.
 - [17] D. Stauffer, *Phys. Repts.* **54**, 1 (1979); D. Stauffer and A. Aharony, *Introduction to Percolation Theory*, Taylor and Francis, London 1994 (revised second edition).
 - [18] H. G. Ballesteros, L. A. Fernandez, V. Martin-Mayor, A. Munoz Sudupe, G. Parisi, and J. J. Ruiz-Lorenzo, *J. Phys. A: Math. Gen.* **30**, 8379 (1997).
 - [19] F. Corberi, E. Lippiello, and M. Zannetti, *Phys. Rev. E* **63**, 061506 (2001); *Eur. Phys. J. B* **24** (2001), 359; *Phys. Rev. E*

- 68**, 046131 (2003); Phys.Rev. E **78**, 011109 (2008); E. Lippiello, F. Corberi, A. Sarracino, and M. Zannetti, Phys. Rev. E **78**, 041120 (2008); F. Corberi, and L.F. Cugliandolo, J. Stat. Mech. P05010 (2009).
- [20] F. Corberi, C. Castellano, E. Lippiello, and M. Zannetti, Phys. Rev. E **65**, 066114 (2002); F. Corberi, E. Lippiello, and M. Zannetti, Eur. Phys. J. B **24** (2001), 359; N. Andrenacci, F. Corberi, and E. Lippiello, Phys. Rev. E **74**, 031111 (2006); E. Lippiello, F. Corberi, and M. Zannetti, Phys. Rev. E **71**, 036104 (2005); R. Burioni, F. Corberi, and A. Vezzani, Phys. Rev. E **79**, 041119 (2009); S. J. Cornell, K. Kaski, and R. B. Stinchcombe, Phys. Rev. B **44**, 12263 (1991).
- [21] S. Puri and N. Parekh, J. Phys. A **26**, 2777 (1993); E. Oguz, A. Chakrabarti, R. Toral and J.D. Gunton, Phys. Rev. B **42**, 704 (1990); E. Oguz, J. Phys. A **27**, 2985 (1994); M. Rao and A. Chakrabarti, Phys. Rev. Lett. **71**, 3501 (1993); C. Aron, C. Chamon, L.F. Cugliandolo and M. Picco, J. Stat. Mech. P05016 (2008). C. Castellano, F. Corberi, U. Marini Bettolo Marconi, and A. Petri, J. Phys. IV France **08**, Pr6-93 (1998).
- [22] H. Park and M. Pleimling, Phys. Rev. B **82**, 144406 (2010).
- [23] F. Corberi, E. Lippiello, and M. Zannetti, Phys. Rev. E **72**, 056103 (2005).
- [24] F. Corberi, E. Lippiello, and M. Zannetti, J. Stat. Mech. P07002 (2007); F. Corberi, E. Lippiello, N. Fusco, and M. Zannetti, Int. J. Mod. Phys. B **18**, 593 (2004); F. Corberi, E. Lippiello, N. Fusco, and M. Zannetti, Physica A **344**, 440 (2004);
- [25] A. Coniglio, Physica A **281**, 129 (2000).
- [26] R. Burioni, F. Corberi, and A. Vezzani, Phys. Rev. E **87**, 032160 (2013); J. Stat. Mech. (2010) P12024; J. Stat. Mech. (2009) P02040; R. Burioni, D. Cassi, F. Corberi, and A. Vezzani, Phys. Rev. E **75**, 011113 (2007); Phys. Rev. Lett. **96**, 235701 (2006).